The Role of Rab32 and Rab38 in Bone Resorption by Osteoclasts

（破骨細胞による骨吸収における Rab32 および Rab38 の役割）

DOCTOR OF PHILOSOPHY

Kanako Tokuda

Center for Frontier Oral Science

Graduate School of Frontier Biosciences

Osaka University

March 2023

Abstract

Osteoclasts play a crucial role in bone homeostasis by forming resorption pits on bone surfaces, resulting in bone resorption. The osteoclast expression of Rab38 protein is highly induced during differentiation from macrophages. Here I generated mice with double knockout (DKO) of Rab38 and its paralogue, Rab32, to investigate the roles of these proteins in osteoclasts. Bone marrow-derived macrophages from Rab32/38 DKO mice differentiated normally into osteoclasts in vitro. However, DKO osteoclasts showed reduced bone resorption activity. These osteoclasts also demonstrated defective secretion of tartrate-resistant acid phosphatase and cathepsin K into the culture medium. In vivo, Rab32 and Rab38 positive cells were attached to the bone surface. Eight-week-old DKO mice showed significantly thickened trabecular bones in micro-CT analysis, as well as reduced serum levels of cross-linked C-telopeptide of type I collagen, indicating diminished bone resorption in vivo. Middle-aged DKO mice (10 to 12 months of age) exhibited kyphosis, which is not usually observed in wild-type male mice until around 24 months of age. These results indicate that Rab32 and Rab38 contribute to osteoclast function by supporting intracellular traffic, thereby maintaining normal bone homeostasis.

Table of contents

Abstract **1**

1. Abbreviation **4**

2. General Introduction **5**

2.1. Bone homeostasis 5

2.2. Character of osteoclasts 6

2.3. Secretory lysosomes and lysosome-related organelle (LRO) 7

2.4. Rab32 and Rab38 proteins 9

3. Introduction of This Thesis **11**

4. Materials and Methods **13**

4.1. Mice 13

4.2. Generation of Rab32/38 DKO mice 13

4.3. Genotyping of Rab32/38 DKO mice 14

4.4. BMM isolation and culture 15

4.5. TRAP staining 16

4.6. Protein extraction and western blotting 16

4.7. Quantitative PCR 18

4.8. Bone resorption assay 19

4.9. TRAP activity assay 19

4.10. CTSK activity assay 20

4.11. 3D micro-CT and bone analysis 20

4.12. Detection of serum C-terminal telopeptides of type I collagen (CTX-I) 21

4.13. H&E and immunofluorescence staining of mouse bone 21

4.14. Statistical analysis 22

5. Results **24**

5.1. Rab32 and Rab38 were expressed in mouse osteoclasts in vivo 24

5.2. Establishment of Rab32/38 DKO mice 24

5.3. Rab32/38 DKO did not affect multinucleated osteoclast formation, CTSK/TRAP production, and osteoclast differentiation marker expression 25

5.4. Osteoclasts from Rab32/Rab38 DKO mice showed reduced bone resorption capacity 27

5.5. TRAP and CTSK secretion efficiency were decreased in osteoclasts of Rab32/38 DKO mice 27

5.6. Rab32/38 DKO mice exhibited increased trabecular bone density 28

5.7. Bone deformation occurred in Rab32/38 DKO mice 28

6. Discussion **30**

7. Figures **34**

8. References **43**

9. Acknowledgments **53**

10. Achievements **55**

10.1. Publications 55

10.2. Meetings 55

1. Abbreviation

BMM: bone marrow-derived macrophage

CTSK: cathepsin K

DGs: dense granules

FBS: fetal bovine serum

FACS: fluorescein amine-labeled chondroitin sulfate

GAPDH: glyceraldehyde-3-phosphate dehydrogenase

GTP: guanine nucleotide triphosphate

GDP: guanine nucleotide diphosphate

H&E: hematoxylin and eosin

HPS: Hermansky-Pudlak syndrome

LRO: lysosome-related organelle

M-CSF: macrophage colony-stimulating factor

NFATc1: nuclear factor of activated T cells c1

RANK: Receptor activator of nuclear factor κ B

RANKL: Receptor activator of nuclear factor κ B ligand

CTX-I: cross-linked C-telopeptide of type I collagen

TRAP: tartrate-resistant acid phosphatase

α-MEM: α-minimum essential medium

micro-CT: micro-computed tomography

2. General Introduction

2.1. Bone homeostasis

Bones play crucial roles in vertebrates including humans, as they structurally support the total body integrity, protect fragile internal organs, enable locomotion together with muscles, and serve as sources of calcium, phosphate, and bone marrow (1). They are porous calcified structures composed of a series of bone-related cells, blood vessels, and bone matrix (1). About 90% of total bone volume is occupied with the bone matrix (2). The bone matrix is composed of the inorganic or mineral matrix (65%), organic matrix (20%), and lipids and water (<15%). The inorganic matrix is composed largely of hydroxyapatite, that is calcium phosphate crystal, and the organic matrix is mostly composed of type I collagen secreted by osteoblasts (2, 3)

Bone maintains its homeostasis by consistently remodeling itself from older to new. Bone remodeling consists of three sequential phases: initiation of bone resorption by osteoclasts, the transition from resorption to the new bone, and bone formation by osteoblasts (4, 5). Bone homeostasis is maintained by a delicate balance between formation and destruction, and accidental imbalance leads to various bone diseases (6). For example, bone resorption by osteoclasts begins to outpace bone formation leading to osteoporosis, which causes bone loss and deterioration of the bone structure, especially in human females after the age of 40 (7). Inflammatory bone disease, rheumatoid arthritis, is characterized by the destruction of articular cartilage and excessive subchondral osteoclastic bone resorption (8). Periodontal disease is another inflammatory bone disease and results from the accumulation of periodontal decomposing bacteria, which activate osteoclasts and destroy the cellular and structural components of periodontal tissue (7). In contrast, osteoclast dysfunction is also associated with diseases of bone (7, 9). When

bone resorption is suppressed by osteoclast dysfunction, it leads to marble bone disease with osteosclerosis (10). Therefore, it would be important for human health to understand the details of osteoclast character as an approach to understanding and overcoming the etiology of these diseases.

2.2. Character of osteoclasts

Osteoclasts are multinucleated giant cells with the monocyte-macrophage lineage that arise by intercellular fusion of macrophages, possessing 2 to several dozen nuclei and ranging from 20 to 100 μm in size (6). Osteoclast proliferation and differentiation are stimulated by extracellular cytokine that regulates the activity of nuclear transcriptional regulators (6). Monocyte- and macrophage-derived osteoclast progenitors receive macrophage colony-stimulating factor (M-CSF), a paracrine factor produced by osteoblasts and osteocytes via a colony-stimulating factor receptor/c-FMS localized on the cell membrane that provides the signal necessary for osteoclast survival and proliferation (11). Receptor activator of nuclear factor κ B ligand (RANKL), also secreted from osteoblasts, binds to receptor activator of nuclear factor κ B (RANK), a membrane receptor expressed on osteoclast precursor cells, recruits tumor necrosis factor (TNF) receptor-associated factor 6 (TRAF6), which in turn recruits downstream NF-κB, c-Jun N-terminal kinase (JNK), p38, and extracellular signal-regulated kinase (SCK), and induces the expression of the extracellular signal-regulated kinase (ERK) pathways (10, 12). In addition, it activates transcription factors such as NF-κB, microphthalmia transcription factor, c-Fos, and nuclear factor-activated T cells c1 (NFATc1) to promote osteoclast differentiation and multinuclear maturation through cell fusion (12, 13).

In the cytoplasm of osteoclasts, there are numerous mitochondria and a developed Golgi apparatus, indicating that osteoclasts are active in energy metabolism and protein synthesis (14, 15). The Golgi apparatus and trans-Golgi network (TGN) reside in proximity to the nucleus, actively involved in lysosome biogenesis and various membrane components. Lysosomes are membrane-bound organelles that contain a variety of soluble acid-hydrolyzing enzymes, highly glycosylated integral membrane protein and degrade materials taken up from inside and outside the cell (16)(17). In addition, many lysosomes, vesicles, and multivesicular bodies are also observed in osteoclasts (14). Osteoclasts exist as attaching to the bone surface, accompanying two structures; the ruffled border characterized by a folded cell membrane structure, and the bright zone that surrounds the ruffled border with actin filaments and adheres to the bone surface, forming a bone resorption pit (18). Vacuolar H^+ -ATPase (V-ATPase), are proton pumps localized on the membrane surface of the ruffled border and acidify the resorption pits (19). The ruffled border and resorption pit are together functionally equivalent to lysosomes in that they contain V-ATPase and hydrolytic enzymes such as cathepsin K and tartrate-resistant acid phosphatase (TRAP), and thereby digest bone matrix in the same way that lysosomes digest incorporated materials (18, 20).

2.3. Secretory lysosomes and lysosome-related organelle (LRO)

In some cells, such as cytotoxic T lymphocytes, mast cells, and osteoclasts, a kind of organelle, secretory lysosomes, exist that can store and release secreted proteins in addition to the conventional degrading function of lysosomes (21)(22). In osteoclasts, it has been reported that cathepsin K and TRAP accumulate within secretory lysosomes and that these organelles fuse with the ruffled border to form active bone resorption pits (23).

The V-ATPase localized on the secretory lysosomal membrane is transported to the ruffled border, acidifying the bone resorption pits, activating hydrolytic enzymes, and degrading bone (24). Secretory lysosomes require further characterization, they may be a type of lysosome-related organelle (LRO), defined as a specialized organelle possessing lysosome-like properties and cell type–specific functions (17). LROs have a structure in common with endosomes and lysosomes, and in addition to lysosomal proteins, include cell type-specific components that perform specialized functions, and are specialized for storage and secretion rather than degradation of their contents (25). LROs are known to function in various processes such as pigmentation, hemostasis, lung homeostasis, and immunity (25). Typical LROs that are well-known include melanosomes, platelet-dense granules (DGs) and lamellar bodies (17)(26). Melanosomes localize to melanocytes and retinal pigment epithelial cells and synthesize and storage a group of related pigments known as melanin, a major factor in defining skin and hair color (17). Melanosomes contain soluble proteins and transmembrane lysosomal proteins (17). DGs are also involved in platelets and megakaryocytes and play a central role in hemostasis and thrombosis. They contain a highly condensed core composed of serotonin, calcium, ATP, ADP, and pyrophosphate, which are important for the fluid coagulation reaction (17). The platelet-dense granule lumen is slightly less acidic than lysosomes and lacks lysosomal hydrolytic enzymes, but contains H^+ pumps, serotonin transporters, and lysosomal proteins (17). Lamellar bodies are localized in type II alveolar epithelial cells, and are composed of surfactant biogenesis of lamellar bodies, LROs involved in storage and secretion of surfactant phospholipids into the alveolar space, reduction of alveolar surface tension, and alveolar dilation (26). Like other LROs, the lumen of the lamellar body is acidified and contains hydrolytic enzymes and lysosomal proteins (26).

2.4. Rab32 and Rab38 proteins

Membrane traffic represents organelle migration, vesicle transport between organelles, vesicle secretion, and autophagy. Rab is a class of small GTPase-family proteins broadly conserved in eukaryotes and functions as the master regulator of membrane traffic (27). Mammals contain approximately 60 different Rab proteins that are supposed to play specialized roles in various cellular processes (28). Rab proteins localize to various organelles and intracellular compartments and work as a molecular switch that regulates intracellular membrane trafficking, including cargo sorting, vesicle formation, vesicle transport, tethering and fusion to specific organelles (29). Rab proteins cycle between GTP-bound active and GDP-bound inactive forms to regulate their functions in membrane traffic and organelle biosynthesis (29).

Several reports have been published on the involvement of Rab in osteoclasts. Rab7, which regulates lysosomal trafficking, is highly expressed in mouse osteoclasts and is involved in an actin ring formation and bone resorption (30) and the regulation of lysosomal trafficking to the ruffled border (31). Rab3DKO mice have increased bone mass and impaired bone resorption capacity due to abnormal formation of the ruffled border (32). Osteoclasts from Rab27A-deficient mice, which are involved in LRO and vesicular trafficking, show abnormal subcellular localization of lysosome-associated membrane protein (LAMP2) and cathepsin K, as well as impaired actin ring formation and bone resorption capacity (33). More than half of Rab proteins are expressed in osteoclasts (34). However, little is known about the function of each Rab protein in osteoclasts.

Rab32 and Rab38 have been reported to play important roles in the regulation of LROs. These two Rab prpteins are approximately 75% identical in sequence, and

Rab32 is broadly expressed while Rab38 is specifically expressed in LRO-containing tissues and cells such as melanocytes and platelets (35). The two proteins have overlapping functions in melanosome biogenesis in melanocytes (36). Both localize on the melanosome membrane and regulate post-Golgi vesicular transport of melanosomal enzymes to immature melanosomes (36–38). Chocolate mice possessing a point mutation in Rab38 show typical characteristics of LRO deficiency, such as impaired melanosome biosynthesis resulting in coat color depigmentation, a marked increase in lung surfactant, and pronounced expansion of the lamellar bodies of the lungs (39, 40). Rab38 is the gene causative of Hermansky-Pudlak syndrome (HPS), in which defective biogenesis of LROs results in an abnormal pulmonary phenotype, predisposition to hemorrhage, and oculocutaneous albinism (41). A mouse model of severe HPS involving Rab32/38 double knockout (DKO) is characterized by atypical coat color, eye pigment dilution, and abnormal lung morphology with reduced numbers of DGs (42). In human platelets, single deletion of Rab38 or Rab32 does not affect DGs biosynthesis or function, indicating that Rab32/38 play redundant roles in the biosynthesis of DGs (42).

3. Introduction of This Thesis

Bone homeostasis, including bone structure and function, is maintained by a delicate balance between bone formation by osteoblasts and bone resorption by osteoclasts (6). Accordingly, several bone-related diseases are associated with osteoclast malfunction: excessive activation of osteoclasts leads to diseases such as osteoporosis, periodontitis, and rheumatoid arthritis, whereas suppression of osteoclast activity and bone resorption leads to conditions involving bone sclerosis, such as marble bone disease (7, 9). Osteoclasts are multinucleated giant cells that originate from the intercellular fusion of monocyte-macrophage lineage cells (6). Osteoclasts differentiate upon stimulation by macrophage colony-stimulating factor (M-CSF) and receptor activator of NF-κB ligand (RANKL), which are paracrine factors produced by osteoblasts and osteocytes (6). Osteoclasts adhere to the bone surface and form a zone termed the ruffled border, characterized by a wavy area of the plasma membrane (18). Ruffled border functions as a secretory organelle for bone resorption in osteoclasts (34). Osteoclasts seal around the ruffled border by actin rings to form bone resorption pits and secrete H^+ and hydrolytic enzymes from the ruffled border to acidify the resorption pit and degrade bone matrix. (19). The ruffled border and resorption pit are together functionally equivalent to lysosomes in that they contain vacuolar H^+-ATPase (V-ATPase) and hydrolytic enzymes such as cathepsin K and tartrate-resistant acid phosphatase (TRAP), and thereby digest bone matrix in the same way that lysosomes digest incorporated materials (18, 20). It has also been reported that cathepsin K and TRAP accumulate within secretory lysosomes in organelles, and that these organelles fuse with the plasma membrane to form active bone resorption pits (23). Although secretory lysosomes require further characterization, they may be considered to be a type of lysosome-related organelle (LRO), defined as a

specialized organelle possessing lysosome-like properties and cell type–specific functions (16, 19). It is supposed that dynamic organelle trafficking and secretion of vesicles containing hydrolytic enzymes, i.e., membrane trafficking, are essential for osteoclasts during differentiation and bone resorption. Membrane trafficking is a mechanism for organelle trafficking, transport of vesicles between organelles or between the plasma membrane and the organelle, and secretion of vesicles to the extracellular cell (43). Rab is a class of small GTPase-family proteins that are broadly conserved in eukaryotes and that function as fundamental regulator of membrane traffic (27). Mammals contain approximately 60 different Rab proteins that are assumed to play specialized roles in various cellular processes (28). Previous reports have indicated that more than half of Rab proteins are expressed in osteoclasts, but very few Rabs have been functionally characterized in osteoclasts (34).

Our laboratory examined the expression of all Rab protein genes in macrophages and osteoclasts using DNA microarray. As a result, Rab38 expression is highly induced during osteoclast differentiation (Noda et al., submitted).

Our laboratory also reported that Rab32 and Rab38 co-localize on LROs in osteoclasts (Noda et al., submitted). However, the role of Rab32/38 in osteoclasts is not clear. In this study, I investigated the role of Rab32/38 in osteoclast function. I generated Rab32/38 DKO mice and evaluated the effects on bone resorption and structural changes.

4. Materials and Methods

4.1. Mice

C57BL/6J mice were purchased from Japan SLC (Shizuoka, Japan). All mice were maintained under specific pathogen–free conditions in the animal facility of the Graduate School of Dentistry, Osaka University. Mice used for isolation of bone marrow cells and collection of femurs, tibias, and fibulas, were appropriately euthanized using carbon dioxide inhalation. Mice used for whole blood collection and micro-CT imaging were euthanized using a mixture of three anesthetics (3% Domitor (medetomidine hydrochloride 1.0 mg/mL, AHD1, ZENOAQ), 8% Dormicum (midazolam 5.0 mg/mL, 17008A2, Astellas), and 10% Betolfal (butorphanol tartrate 5.0 mg/mL, VETLI5, Meiji Seika) in MilliQ water). This mixture was administered intraperitoneally at a dose of 0.1 mL per 10 g of body weight. All animal studies were approved by the Institutional Animal Experiments Committee of Osaka University Graduate School of Dentistry (29-008-0) and the Gene Modification Experiments Safety Committee of Osaka University.

4.2. Generation of Rab32/38 DKO mice

The CRISPR/Cas9 system was injected into mouse embryos by electroporation at the Institute of Experimental Animal Sciences, Osaka University Medical School, as previously reported (44). The guide RNAs were designed to target the Rab32 exon 1 and Rab38 exon 1 loci (Figure 2A). F_0 mosaic mutant mice were crossed with C57BL/6J mice to produce heterozygous mice with a 4-nucleotide base-pair deletion in Rab32 and a 5-nucleotide base-pair deletion in Rab38 in F_1 mice. Generation of F_1 mice was confirmed by Sanger sequencing, with DNA collected from mouse ears used as a PCR template. Primers used for PCR and Sanger sequence analysis are as follows. Rab32:

GGTAGCCAGGGAAGAGGAAG (Forward) and ACCGGGAGACAGAGAGGAGT (Reverse), Rab38: GCACCAGCTCCCTATCCTG (Forward) and ACTCCTCACTGGCTCACTCC (Reverse). The resulting F1 heterozygous mutant mice were crossed with WT mice to obtain F2 heterozygous mutant mice. Furthermore, F1 heterozygous mutant mice were crossed with F2 heterozygous mutant mice to obtain F3 homozygous mutant mice. Homozygous mutant mice were then crossed with each other to maintain the Rab32/38 DKO mouse line.

4.3. Genotyping of Rab32/38 DKO mice

DNA was extracted from mouse ear specimens using the KAPA Express Extract Kit (Roche) and purified by isopropanol precipitation. PCR was performed using Tks Gflex DNA Polymerase (Takara Bio) with initial denaturation at 94 °C for 1 min, followed by 40 cycles of denaturation at 98 °C for 10 s, annealing at 60 °C for 15 s, and elongation at 68 °C for 30 s. The resulting PCR products were mixed with the gel loading dye. Generation of 15% polyacrylamide gel was performed by mixing 40%(w/v) -acrylamide/bis mixed solution (19:1) (Nacalai Tesque), 5 X TBE (44.5 mM Tris-borate (pH 8.3), 10 mM EDTA), 10% ammonium persulfate, and TEMED, and poured in a slab gel plate. After electrophoresis using 1 X TBE as buffer at 40 mA for 2 h, the polyacrylamide gel was immersed in a 0.5 μg/mL ethidium bromide solution for 10 min and detected using DigiDoc-It Darkroom (UVP). The following primers were used for genotyping. Rab32 : CGAGGGACTAGGGCAACAG (Forward) and AAAGAGGTGCTCTCGGGTC (Reverse), Rab38: ACAAGGAGCACCTGTACAAG (Forward) and AGCGCTTGATAATGCTGGTC (Reverse).

4.4. BMM isolation and culture

Male C57BL6J mice or Rab32/38 DKO mice between 7 and 10 weeks of age were used for the experiments. Under aseptic conditions, the femurs and tibias of mice were harvested and the medullary cavity of the bones was rinsed with α-MEM with L-glutamine and phenol red (135-15175, Fujifilm Wako Pure Chemical Corporation) containing 60 μg/mL kanamycin (Fujifilm Wako Pure Chemical Corporation) in a 5-mL syringe and centrifuged at 250 x g for 5 min. Red blood cell lysing buffer (150 mM NH_4Cl, 10 mM $KHCO_3$, 0.1 mM EDTA (pH 7.4)) was added to remove blood cells, and the remaining cells were used as bone marrow cells. These cells were suspended in 10 mL of α-MEM basal medium (α-MEM with L-glutamine and phenol red containing 60 μg/mL kanamycin and 10% FBS), seeded into 100-mm petri dishes, and cultured in 5% CO_2 at 37 °C overnight. As the M-CSF conditioned medium, the culture supernatant of CMG14-12 cells, a mouse M-CSF–producing Ltk- cell line, was collected in α-MEM basal medium (45). After 10-h incubation, non-adherent cells in the supernatant were collected and seeded in 24-well plates (2.5×10^5 cells/well), 48-well plates (1.0×10^5 cells/well), or 96-well plates (4.0×10^4 cells/well) in α-MEM basal medium with 10% M-CSF conditioned medium. After 48-h culture, adherent cells were defined as BMMs and were replaced with differentiation medium (α-MEM basal medium, 2% M-CSF conditioned medium, and 400 ng/ml GST-RANKL, prepared as previously described (46) to induce differentiation into osteoclasts. This point was designated as culture day 0. After 3 days, half of the medium was replaced and osteoclasts were collected at 5 or 6 days of differentiation (47, 48).

4.5. TRAP staining

TRAP staining was performed using a TRAP Staining Kit (AK04F, Cosmo Bio). Bone marrow derived from the femurs and tibias of WT and Rab32/38 DKO mice was harvested in 96-well plates and cultured in α-MEM basal medium with M-CSF for 2 days to induce BMMs. Then, RANKL was added and culture was performed for 5 days to induce differentiation into osteoclasts. Osteoclasts on 96-well plates were fixed in 10% Formalin Neutral Buffer Solution and incubated with Chromogenic Substrate Solution at 37 °C for 20-60 min. Once sufficiently colored, the reaction was stopped by washing the wells with pure water. TRAP-positive multinucleated cells (three or more nuclei) were counted as differentiated osteoclasts.

4.6. Protein extraction and western blotting

Osteoclast differentiation was induced in differentiation medium for 5 or 6 days in 24-well plates. Cells were then washed with PBS (137 mM NaCl, 2.7 mM KCl, 10 mM Na_2HPO_4, 1.76 mM KH_2PO_4 (pH 7.4)), and 50 μL lysis buffer (50 mM Tris-HCl (pH 7.5), 150 mM NaCl, 1% TritonX-100, EDTA-free Protease Inhibitor Cocktail Tablets (Roche)) was added to each well. After the plates were allowed to stand for 10 min on ice, the whole-cell lysate was collected, and 6 wells were combined into one sample. After centrifugation at 20,400 x g for 10 min, supernatants were collected and then protein quantification was performed by Pierce Coomassie Plus (Bradford) Assay Kit (Thermo Fisher). Protein concentrations were adjusted to 1 mg/mL.

For protein extracts from mouse organs, small samples of tissue were washed in PBS and placed in one well in the 6-well plate containing 1 mL lysis buffer, and stainless mesh (40 mesh/inch, E9111, Q-ho Metal Works) was placed over the tissue on

ice and pushed through it using a 5-mL syringe plunger head. The whole-tissue lysate was collected into 1.5 mL tubes, stored at -80 ℃ overnight, and then stored at 4 ℃ until totally thawed. This freeze-and-thaw step was repeated twice, and protein extracts were collected after centrifugation as described above. Protein concentrations were adjusted to 5 mg/mL.

The samples were suspended in sample buffer (300 mM Tris-HCl (pH 6.8), 12% SDS, 30% glycerol, 0.006% bromophenol blue, 0.6 M 2-mercaptoethanol) and boiled for 3 min. Ten micrograms of protein from cell samples or 50 μg of protein from tissue samples were electrophoresed in SDS-PAGE using 15% polyacrylamide gel and running buffer (25 mM Tris-HCl (pH 8.3), 191 mM glycine, 0.1% SDS). The proteins were transferred to polyvinylidenefluoride (PVDF) membranes (GE Healthcare) using transfer buffer (25 mM Tris-HCl (pH 8.3), 192 mM glycine, 20% methanol) in a transfer device (NA-150: Nihon Eido) (100 V, 150 mA, 1 hr). PVDF membranes were treated with PBS-T (3.2 mM Na_2HPO_4, 0.5 mM KH_2PO_4, 1.3 mM KCl, 135 mM NaCl, 0.05% Tween 20 (pH 7.4)) containing 5% skim milk (Morinaga Milk Industry) for 60 min at room temperature for blocking. The primary antibody was reacted with a diluted solution of Can Get Signal (TOYOBO) Solution I for 1 h at room temperature, followed by washing with PBS-T for 15 min. Then, the secondary antibody was reacted with a solution diluted with Can Get Signal (TOYOBO) Solution II for 1 h at room temperature, followed by washing in PBS-T for 15 min. After washing, the membrane was reacted with ECL Select Western Blotting Detection Reagent (GE Healthcare), and bands were detected using Gene Gnome 5 (Syngene). The dilution ratio of each antibody was as follows: primary antibodies were anti-Rab32 rabbit (49): 1/1000, anti-Rab38 rabbit (49): 1/1000, anti-cathepsin K (sc-48353, E-7, Santa Cruz): 1/200, anti-GAPDH (2275-PC-100, R&D

system): 1/5000 and anti-tubulin (T9026, Sigma): 1/10000; secondary antibodies were anti-rabbit IgG HRP (CST): 1/2000 and anti-mouse IgG HRP (Southern Biotech): 1/10000.

4.7. Quantitative PCR

Total RNA of BMMs and osteoclasts cultured in 24-well plates was extracted using TRIsure (Bioline). The extracted RNA was used as a template for reverse transcription using the iScript cDNA Synthesis Kit (Bio-Rad) to generate complementary strand DNA (cDNA). Real-time PCR analysis was performed using QuantiTect SYBR Green PCR (Qiagen), with the following cDNA used as templates and primers for genes specific for osteoclast differentiation. GAPDH: AAATGGTGAAGGTCGGTGTG (Forward), TGAAGGGGTCGTTGATGG (Reverse), CTSK: GCCAGGATGAAAGTTGTATG (Forward) CAGGCGTTGTTCTTATTCC (Reverse), TRAP: GCTGGAAACCATGATCACCT (Forward) GAGTTGCCACACAGCATCAC (Reverse), DC-STAMP: TGTATCGGCTCATCTCCTCCAT (Forward) GACTCCTTGGGTTCCTTGCTT (Reverse). The Step One Plus Real-time PCR System (Applied Biosystems) was used for reaction and detection. Relative gene expression levels for each gene were calculated according to the ΔΔCt method (50), using GAPDH as the internal control gene. The fold induction of osteoclast marker genes was normalized to the basal levels in BMMs, and then the fold induction of mRNA was compared between WT and Rab32/38 DKO osteoclasts.

4.8. Bone resorption assay

Bone resorption activity was evaluated using a Bone Resorption Assay Kit (BRA-24kit, PG Research). Bone marrow derived from femurs and tibias of WT and Rab32/38 DKO mice was cultured on a FACS/calcium phosphate–coated 48-well plate in α-MEM basal medium with M-CSF for 2 days to induce BMMs. Then, BMMs were induced to differentiate into osteoclasts using differentiation medium without phenol red for 5 days, and the culture supernatant was collected. The fluorescence intensity of the collected supernatant was measured at an excitation wavelength of 485 nm and an emission wavelength of 535 nm by Twinkle LB 970 (Berthold), a microplate reader. For pit area analysis, each well was treated with 2.5% sodium hypochlorite for 5 min to remove cells, then the wells were washed with distilled water and dried. Each well was randomly photographed under an optical microscope with a 10 x objective, and the total pit area per image was measured using ImageJ software. In brief, I drew the outline of each pit area and measured the number of pixels per area. All pixels from one image were summed up, and 6 images per well and 3 wells per condition were analyzed.

4.9. TRAP activity assay

Osteoclasts were prepared in 96-well plates by phenol-red free differentiation medium. The culture supernatants were collected and diluted 5-fold by TRAP activity assay buffer (TAAB) (1 mM ascorbic acid, 0.1 mM $FeSO_4$-$7H_2O$, 0.1 mM $(NH_4)_2SO_4$, 0.1 M sodium acetate, 0.15 M KCl, 10 mM sodium (+)-tartrate dihydrate, 0.1% Triton-X100 (pH 5.8)). Cell pellets were washed twice by PBS, lysed by 100 μL TAAB on ice for 10 min, and further diluted 10-fold in TAAB buffer. Ten μL of TRAP substrate (100 mM *p*-nitrophenylphosphoric acid disodium salt (25019-52, Nacalai Tesque) dissolved in

TAAB) was added into 200 μL of diluted supernatant or cell lysate and incubated for 10 min at 37 °C, then 50 μL of 0.5 M NaOH was added to stop the reaction. Absorbance at 405 nm was measured by iMark (Bio-Rad). The assay background was cell-free medium or TAAB buffer.

4.10. CTSK activity assay

CTSK activity in cell culture supernatants and cell lysates was detected by Magic Red-Cathepsin K (#6135, ImmunoChemistry Technologies). Osteoclasts were prepared with phenol-red free differentiation medium in 24-well plates. To collect CTSK, 300 μL fresh differentiation medium was directly added into each well every 3 days without removing culture medium. Cell supernatants were collected 9 days after differentiation induction, and cell pellets were washed twice with PBS and lysed with 1% Triton-X100, 150 mM NaCl, 50 mM Tris-HCl (pH 7.8). Magic Red staining solution in DMSO was diluted 10-fold in H_2O and 8 μL was added to 200 μl of supernatant or cell lysate. After 15-min incubation at room temperature, fluorescence signals (Ex. 530 nm, Em. 590 nm) were detected by the PowerScan HT fluorescence microplate reader (BioTek DS Pharma Biomedical). Medium or lysis buffer was used as background control.

4.11. 3D micro-CT and bone analysis

For 3D analysis of bone, the distal end of the femur of an 8-week-old male mouse was used to acquire images using a 3D micro-CT scanner R_mCT2 (Rigaku) with the X-ray source conditions set to 60 kV voltage, 120 μA current, and FOV of 10. The trabecular bone near the distal growth plate of the femur was then reconstructed three dimensionally using TRI/3D-Bone software (Ratoc) and the following parameters were analyzed: bone

volume per tissue volume: BV/TV (%), trabecular thickness: Tb. Th (μm), bone mineral content per tissue volume: BMC/TV (mg/cm^3), trabecular number: Tb. N (1/mm) and trabecular separation: Tb.Sp (μm).

Mouse spines were analyzed using 8-week-old or 10- to 12-month-old male mice. For spine kyphosis analysis, a 3D micro-CT scanner was used to acquire images of the cervical to the thoracic spine after mice were completely anesthetized. Scanning conditions were as follows: FOV, 60; acquisition time, fine 2 min. The distance AB was defined as that between the caudal margin of the last cervical vertebra and the caudal margin of the sixth lumbar vertebra. The distance CD was defined as that from the dorsal edge of the vertebra at the point of greatest curvature to a point perpendicular to the line AB. The kyphosis index was the distance AB divided by the distance CD (51).

4.12. Detection of serum C-terminal telopeptides of type I collagen (CTX-I)

Whole blood was collected from 8-week-old WT and Rab32/Rab38 DKO male mice. The blood was placed at room temperature for 30 min and then centrifuged at 16,300 x g at 4 ºC for 10 min. The supernatants were collected and used immediately or stored at -80 ºC. CTX-I in 20 μL serum per test were detected by a Rat-Laps (CTX-I) EIA kit (AC-06F1, Immunodiagnostic Systems). In the final step, the absorbance at 450 nm and the reference absorbance at 570 nm was measured by iMark (Bio-Rad).

4.13. H&E and immunofluorescence staining of mouse bone

Fluorescence immunostaining and H&E staining and image superimposition were performed as previously reported (52). Femurs were harvested from 8-week-old male WT mice, fixed in 4% paraformaldehyde (PFA) at 4 °C overnight, and demineralized in 10%

EDTA (pH 7.0) for 14 days. Demineralized bone tissue was embedded in paraffin and sectioned at 4-μm thickness using a Leica CM1850 (Leica Biosystems). Formalin-fixed, paraffin-embedded (FFPE) sections were mounted on glass slides and dried at 40 °C overnight. Then, the FFPE sections were baked for 1 h at 60 °C. Paraffin was then removed from the FFPE sections using xylene and ethanol sequentially (100%, 100%, 90%, 80%, 70%, each 10 min) using ASP300S (Leica Biosystems), and rinsed in water for rehydration. To block endogenous peroxidase activity, the tissue sections were soaked with 3% H_2O_2 in methanol for 10 min. To block nonspecific binding, tissue sections were incubated in 5% BSA and 1% goat serum in PBS for 30 min at room temperature. After that, sections were incubated with primary antibody (diluted in 1% BSA in PBS) at 4 °C overnight. On the next day, the secondary antibody was treated at room temperature for 1 h. Finally, mounting medium was added to the slide and topped with a coverslip. The dilution ratio of each antibody is as follows: primary antibodies were anti-Rab32 rabbit (49): 1/500 and anti-Rab38 rabbit (49): 1/500; the secondary antibodies were Alexa Fluor 488–conjugated anti-rabbit (Thermo Fisher Scientific). The coverslip of the section was gently removed by soaking in PBS followed by standard hematoxylin and eosin (H&E) staining (53). Adobe Photoshop software (CS6, Adobe Systems, San Jose, CA) was used to superimpose the histochemical staining image (x 400; DS-Ri2, Nikon) onto fluorescence images (TSC SP8, Leica).

4.14. Statistical analysis

Data were analyzed with Graph Pad Prism version 7.04. All data are expressed as mean ± standard deviation (SD). Data comparisons between two groups were analyzed using

the unpaired Student t-test; P-values less than 0.05 were considered statistically significant. * $P<0.05$, ** $P<0.01$, and *** $P<0.005$.

5. Results

5.1. Rab32 and Rab38 were expressed in mouse osteoclasts in vivo

In the previous paper by Noda et al, the expression of Rab32 and Rab38 were validated in osteoclast induced from macro bone marrow-derived macrophage in vitro (Noda et al, submitted). To further study the expression of Rab32 and Rab38 in vivo, I first examined the localization of these molecules inside bone tissues. Fluorescence immunostaining for Rab32 or Rab38 was performed on femur tissue sections prepared from 8-week-old WT mice, and followed by hematoxylin and eosin (H&E) staining. Rab32 was detected at the contact areas between the bone and attached cells, and Rab38 appeared in similar areas. Rab32 exhibited significant accumulation in the bone surface, whereas Rab38 showed a wider distribution within the attached cells (Figure 1A, B). Both Rab32 and Rab38 positive signals were scarce inside the bone matrix (Figure 1A, B). These images are consistent with the view that Rab32 and Rab38 are expressed in osteoclasts in vivo.

5.2. Establishment of Rab32/38 DKO mice

To investigate the role of Rab32 and Rab38 in osteoclast function, Rab32/38 DKO mice were generated from C57BL6/J mice using the CRISPR/Cas9 system. Guide RNAs were designed to target the Rab32 exon 1 and Rab38 exon 1 loci (Figure 2A). F_0 mosaic mutant mice were crossed with C57BL/6J mice to produce F_1 progenies heterozygous for a 4-nucleotide base-pair deletion in Rab32 and a 5-nucleotide base-pair deletion in Rab38. The mutations were confirmed by DNA sequencing, and they were considered to be null alleles because they cause frame shifts of the reading frames encoded in exon 1 (Figure 2B). Each offspring was genotyped by specific PCR of their genome (Figure 3A). The resulting F1 heterozygous mutant mice were crossed with WT mice to obtain F2

heterozygous mutant mice. Furthermore, F1 heterozygous mutant mice were crossed with F2 heterozygous mutant mice to obtain F3 homozygous mutant mice. Thereafter, homozygous mutant mice were crossed with each other after 8 weeks of age to maintain the Rab32/38 DKO mouse line.

The protein extracts from mouse tissues, including the heart, spleen, lung, liver, and kidney, were subjected to western blotting with anti-Rab32 and -Rab38 antibodies. Rab32 signals were detected in the spleen, lung, and liver in WT mice but not in Rab32/38 DKO mice (Figure 3B). Rab38 signals were barely detectable in any of these organs, even in WT mice, implying relatively low expression of Rab38 in these tissues (data not shown).

Of note, Rab32/38 DKO mice exhibited a light beige coat and red eyes, compared to the black coat and black eyes of C57BL6/J wild-type mice (Figure 4A, B). This is consistent with the recently reported phenotype of Rab32/38 DKO mice (42). While Rab32 single knockout mice showed no apparent difference compared to wild-type mice in either coat or eye color, both their coats and eyes did have a slight pigment deficiency that was also seen in a chocolate mouse mutant with a Rab38 natural point mutation (54) (data not shown). These phenotypes were consistent with previous reports showing crucial overlapping roles of Rab32/38 in melanosome biogenesis (36, 42), and supported the successful establishment of the Rab32/38 mutant mouse line.

5.3. Rab32/38 DKO did not affect multinucleated osteoclast formation, CTSK/TRAP production, and osteoclast differentiation marker expression

Next, the effect of Rab32/38 DKO on bone marrow-derived macrophage (BMM) differentiation into osteoclasts was evaluated. Bone marrow from the femurs and tibias

of WT and Rab32/38 DKO mice was harvested and cultured with M-CSF for 2 days, then cultured with RANKL for 5 or 6 days to induce differentiation into osteoclasts. The mRNA expression of dendritic cell-specific transmembrane protein (DC-STAMP), tartrate-resistant acid phosphatase (TRAP), and cathepsin K (CTSK), which are induced during BMM differentiation into osteoclasts (55–57), were measured by qPCR. The induction levels of these genes in DKO osteoclasts were indistinguishable from those in WT cells (Figure 5A).

The total intracellular protein extracts from BMMs and osteoclasts derived from WT and Rab32/38 DKO mice were subjected to western blotting. As reported, Rab32 protein was expressed in WT BMMs and osteoclasts, whereas Rab38 was absent in WT BMMs (Figure 5B) (Noda et al., submitted). Neither Rab32 nor Rab38 was detected in Rab32/38 DKO osteoclasts or BMMs, further confirming the establishment of null mutants of Rab32 and Rab38 (Figure 5B). When the protein extracts from BMMs and osteoclasts of WT and Rab32/38 DKO mice were probed with anti-CTSK antibody, the CTSK signal was highly induced in differentiated DKO osteoclasts as well as WT osteoclasts (Figure 5B).

Furthermore, I quantified the number of TRAP-positive multinucleated cells (MNCs) with more than three nuclei per cell, which correspond to osteoclasts, after 5-day culture with RANKL. WT and Rab32/38 DKO mice exhibited no significant difference in the formation of multinucleated osteoclasts (Figure 5C). Collectively, Rab32/38 DKO had negligible effects on intercellular fusion and multinucleation, CTSK/TRAP generation, and osteoclast differentiation marker expression.

5.4. Osteoclasts from Rab32/Rab38 DKO mice showed reduced bone resorption capacity

I next assessed the bone resorption capacity of osteoclasts derived from Rab32/38 DKO mice. Osteoclasts from WT and DKO mice were cultured for 5 days on culture plates coated with fluorescein amine-labeled chondroitin sulfate (FACS)–bound calcium phosphate, which is subjected to osteoclast enzyme digestion. The digested pit area was significantly smaller in osteoclasts derived from Rab32/38 DKO mice compared to those from WT mice (Figure 6A, B). The cleaved FACS products released into the medium were measured by fluorescence analysis and also significantly reduced in Rab32/38 DKO osteoclasts (Figure 6C). Collectively, Rab32/38 DKO derived osteoclasts have significantly reduced bone resorption capacity.

5.5. TRAP and CTSK secretion efficiency were decreased in osteoclasts of Rab32/38 DKO mice

Various enzymes in osteoclasts, including TRAP and CTSK, are secreted into the resorption pits via vesicular transport (19). First, the distribution of TRAP activity in osteoclast culture was examined. Intracellular TRAP activity was comparable between WT and Rab32/38 DKO osteoclasts (Figure 7A), which is consistent with the data that the two cell types showed similar TRAP mRNA expression and TRAP staining intensity (Figure 5A and C). However, the extracellular TRAP activity in the culture medium was significantly reduced in Rab32/38 DKO osteoclasts (Figure 7B).

Next, the distribution of CTSK activity using a Magic Red Cathepsin K Assay Kit was examined. Similar to the TRAP results, CTSK activity within osteoclasts was similar between WT and Rab32/38 DKO mice (Figure 7C), reflecting equivalent CTSK mRNA expression (Figure 5A) and protein levels (Figure 5B). By contrast, extracellular

CTSK activity in the culture medium was decreased in Rab32/38 DKO osteoclasts (Figure 7D). These results indicate that the secretion of TRAP and CTSK to the extracellular space was hampered in Rab32/38 DKO osteoclasts.

5.6. Rab32/38 DKO mice exhibited increased trabecular bone density

To examine the effect of Rab32 and Rab38 ablation in bone, the serum levels of carboxy-terminal collagen I (CTX-I) crosslinks; these are released as a result of bone resorption and represent osteoclastic activity in vivo (58). The serum CTX-I ELISA level in vivo was significantly lower in Rab32/38 DKO mice than in WT mice (Figure 8A), suggesting that osteoclasia is abrogated in Rab32/38 DKO mice in vivo.

The femurs of 8-week-old male WT and Rab32/38 DKO mice were analyzed using micro-CT. The 3D reconstituted images of trabecular bone in Rab32/38 DKO mice showed a significantly more dense trabecular bone structure than in WT mice (Figure 8B). Indeed, increases in four trabecular bone structure parameters, namely bone volume per tissue volume (BV/TV), trabecular thickness (Tb. Th), bone mineral content per tissue volume (BMC/TV) and trabecular number (Tb. N), as well as a decrease in trabecular separation (Tb. Sp), were observed implying that osteogenesis predominates over osteoclasia in the trabecular bone of Rab32/38 DKO mice (Figure 8C). In contrast, significant differences were not observed in length between WT and Rab32/38 DKO mice femur (Figure 8D).

5.7. Bone deformation occurred in Rab32/38 DKO mice

As described above, there were differences regarding bone indices between WT and Rab32/38 DKO mice at 8 weeks of age, while no clear discrepancy was observed in external appearance at this stage. However, middle-aged (10- to 12-month-old) Rab32/38

DKO male mice showed increased curvature between the beginning of the first thoracic vertebra and the end of the last lumbar vertebra, called kyphosis (Figure 9A). This kyphosis is usually observed in older WT male mice, likely those aged 24 months (59). The kyphosis index (60), representing the degree of curvature, was shown to be significantly decreased in Rab32/38 DKO male mice compared to WT (Figure 9B). This phenotype was absent in females (data not shown). These results indicate that bone homeostasis is disturbed in Rab32/38 DKO, especially in aged male mice.

6. Discussion

In the present study, I showed that Rab32 and Rab38 are required for sufficient activity of bone resorption in osteoclasts. Deficiency of Rab32 and Rab38 increases trabecular bone mass, and in male mice, it results in bone structure abnormalities that become more pronounced with age.

Since Rab38 expression is markedly induced following osteoclast differentiation (61) (Noda et al, submitted), it is possible that Rab38 affects osteoclast differentiation. However, the expression of specific markers for osteoclast differentiation in osteoclasts derived from Rab32/38 DKO mice did not differ from those derived from WT mice, indicating that Rab32/38 DKO cells can differentiate normally into multinucleated osteoclasts containing bone resorption enzymes. In contrast, osteoclasts from Rab32/38 DKO mice had significantly reduced bone resorption capacity. Our results suggest that the loss of bone resorption function resulting from Rab32/38 DKO may be due to defective trafficking of TRAP, CTSK, and V-ATPase to the extracellular space and plasma membrane, which together are equivalent to the resorption pit. In addition, preliminary results suggest abnormal actin ring formation (data not shown). As a result, I suggest that bone resorption functionality in the pit area is severely defective in Rab32/38 DKO mice. It was reported that osteoclasts exist in one of two states: an active state, involving attachment to the bone surface with subsequent bone resorption, and a resting state, marked by detachment from the bone (51). It would be interesting to investigate whether the transition between these two states is altered in Rab32/38 DKO osteoclasts. The increased bone mass in Rab32/38 DKO mice indicates that bone formation predominates over bone destruction in the balance of bone homeostasis. The dysfunctional bone resorption in osteoclasts from Rab32/38 DKO mice is at least one of

the critical factors underlying the increased bone mass in these animals. Since I focused on osteoclasts in this study, I was unable to prove that Rab32 and Rab38 are associated with bone formation by osteoblasts, although I did find that they were present in very low numbers inside the bone matrix in situ. Further studies are needed to clarify this issue, particularly since it has recently become evident that osteoblasts and osteoclasts are regulated by mutual feedback (62).

It has been reported that there are no abnormalities in bone formation in chocolate mice, which harbor a point mutation in Rab38 (54). It should be noted that there is no difference between the coat color of Rab38 null mutant mice (Figure. 1) and that of chocolate mice. The remarkable bone-related phenotype of our Rab32/38 DKO mice indicates that Rab32 and Rab38 function redundantly in osteoclasts, just as they do in melanosomes and dense granule biogenesis (42, 63). V-ATPase a3 subunit KO mouse had an abnormal bone phenotype but a normal melanosome phenotype, even though a3 was localized on melanosomes in WT mice (31, 64, 65). Rab32/38 DKO mice demonstrated both bone and melanosome-related phenotype abnormalities, clearly establishing the relevance of osteoclasts and melanosomes in terms of LRO function. Rab32 single KO mice did not show an abnormal color phenotype, suggesting that Rab38 possesses greater influence over melanosome biogenesis. Rab32 and Rab38 have similar mRNA expression levels after osteoclast differentiation (Noda et al, submitted), so it is reasonable that both are important in osteoclast function. Meanwhile, the lack of an abnormal bone-related phenotype in chocolate mice suggests that Rab32 alone can fulfill most osteoclast-related functions (54). Therefore, it remains unclear why Rab38 is acutely induced during osteoclast differentiation, and the specific role of this protein should be investigated.

The paper by Noda et al. reports that Rab32 and Rab38 co-localize to a novel osteoclast-specific LRO (Noda et al., submitted). In this study, I show that Rab32 and Rab38 are involved in the expression of osteoclast function. Some Rab32 and Rab38 positive LROs are located in close proximity to resorption pits in osteoclasts, and CTSK and TRAP are contained within the LROs of mononuclear osteoclasts after RANKL stimulation (Noda et al., submitted). The Rab32 and Rab38 positive LRO is also positive for V-ATPase. These LROs are at or near the final stage of trafficking to the ruffled border. Based on these observations, I suggest that Rab32/38 DKO does not support the proper function of these enzymes, leading to reduced bone resorption. Rab7 and Rab27 are known to be involved in vesicle trafficking in osteoclasts (33, 66). In particular, V-ATPase plays a crucial role in recruiting Rab7, together with its GEF Mon1-Ccz1, to this LRO (31, 67), and therefore it is highly probable that Rab7 recruitment is disturbed in Rab32/38 DKO osteoclasts. The involvement of these Rab proteins in the Rab32- and Rab38-positive LRO should be clarified in the future.

This study revealed abnormal hyperplasia of the fibula in male mice, possibly caused by an increase in bone mass associated with osteoclast dysfunction. Furthermore, middle-aged male mice exhibited extreme kyphosis, which is usually observed in much older male mice (68). Although the cause of this phenotype is not clearly understood, it seems to share some characteristics with the phenotype known as diffuse idiopathic skeletal hyperostosis, a disease that causes bone hyperplasia of the spine, especially in middle-aged and older human males (69). The kyphotic phenotype that I observed may also be caused by osteoclast dysfunction. The phenotypes characterized by fibular and spinal abnormalities in Rab32/38 DKO mice were observed only in males and not in females. It is conceivable that bone loss progresses with age in C57BL/6J mice just like

in humans (70, 71), and its magnitude is influenced by gender (72). Sex hormones probably also play a role, since they affect osteoporosis and other bone-related phenomena as well (73). For example, it is known that bone mass is generally higher in male mice due to the activation of osteoblasts via androgen receptors (48). This may be the reason why only males showed an increase in bone mass, assuming that osteoclast function was equally impaired in both male and female Rab32/38 DKO mice.

In this study, I revealed that Rab32 and Rab38 are crucial for proper bone formation. Our results indicate that both Rab32 and Rab38 may serve as drug targets for suppressing osteoclast function and may be developed like a bisphosphonate or like odanacatib, a CTSK inhibitor, as a therapeutic agent for rheumatoid arthritis, osteoporosis, and periodontitis (7, 74, 75).

7. Figures

Figure 1

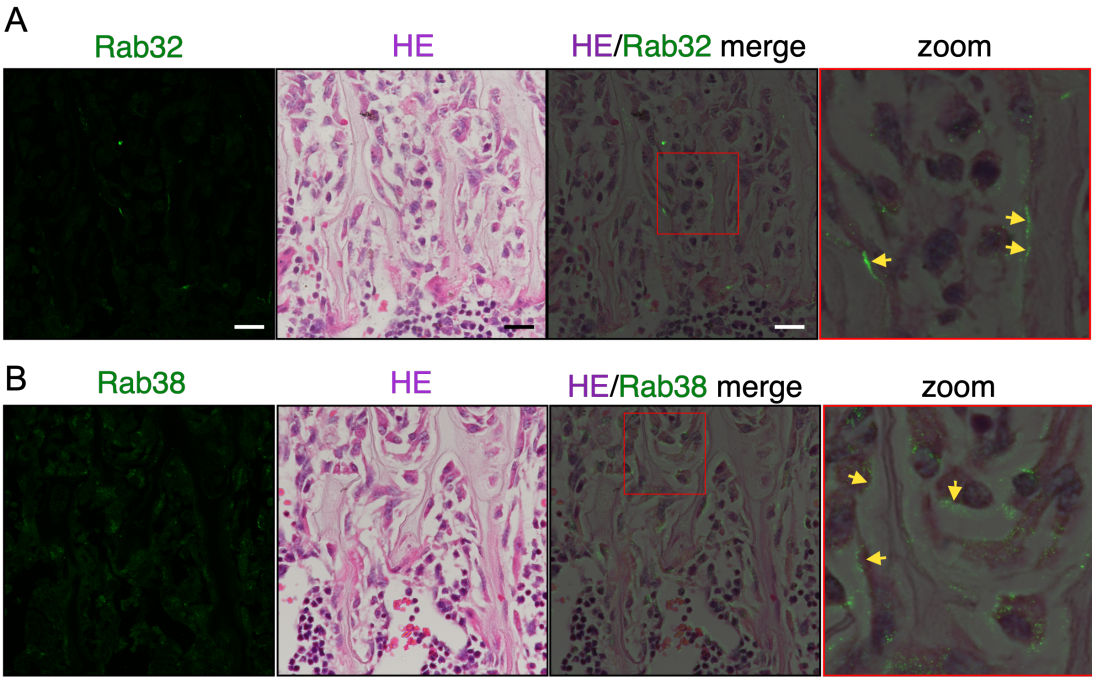

Rab32 and Rab38 are expressed in the osteoclasts of mouse bone.

(**A**) (**B**) H&E and immunofluorescence staining of mouse bones. Femurs were harvested from 8-week-old male WT mice and processed for section preparation as described in the materials and methods. Sections were stained with anti-Rab32 rabbit or anti-Rab38 rabbit polyclonal antibodies, with Alexa Fluor 488–conjugated anti-rabbit IgG as the secondary antibody. After observation of Rab32 and Rab38 signals with a confocal laser scanning microscope, the specimens were further stained with H&E. Fluorescence H&E images were superimposed. Scale bar: 20 μm.

Figure 2

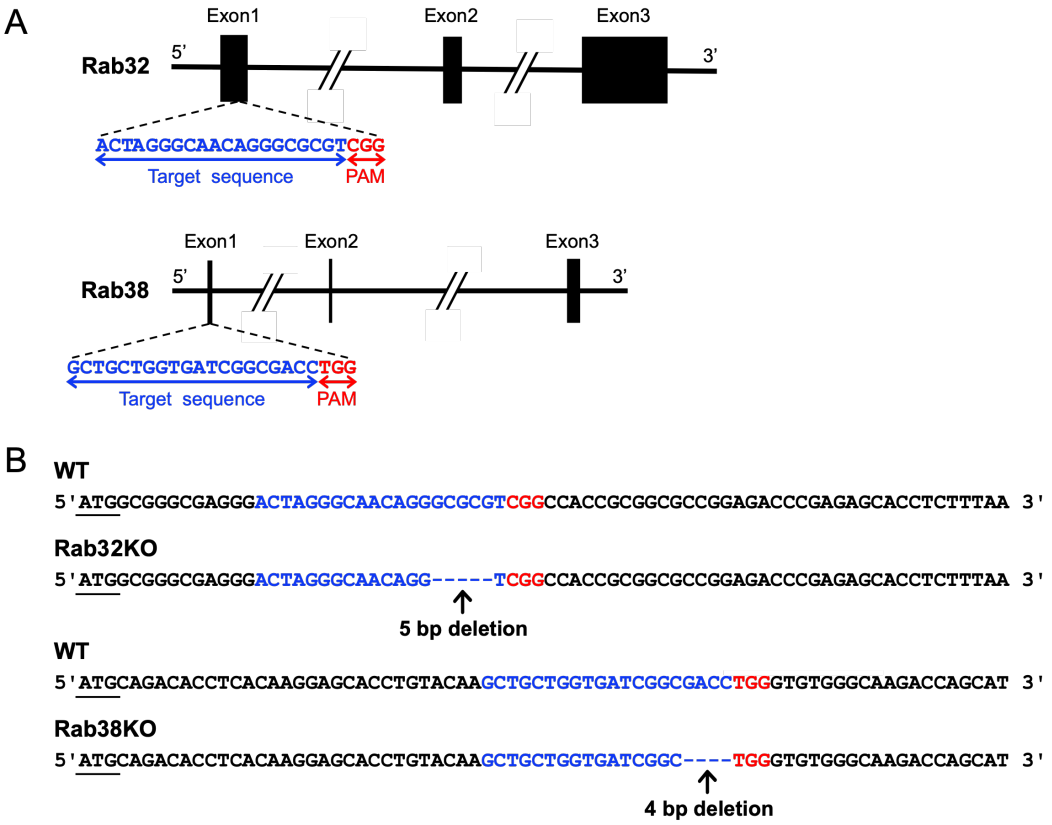

Generation of Rab32/38 DKO mice by CRISPR/Cas9 system.

(**A**) Schematic of the genome loci of Rab32 and Rab38 with the respective target sites of CRISPR/Cas9. Guide RNAs were designed to target the exon 1 loci for both Rab32 and Rab38. Target sites are shown in blue, and protospacer adjacent motif (PAM) sequences are shown in red. (**B**) Targeted genome sequences of Rab32 and Rab38 in WT and Rab32/38DKO mice. Rab32 KO were deleted of 5 base pairs and Rab38 KO were deleted of 4 base pairs, respectively. Initiation codons are underlined.

Figure 3

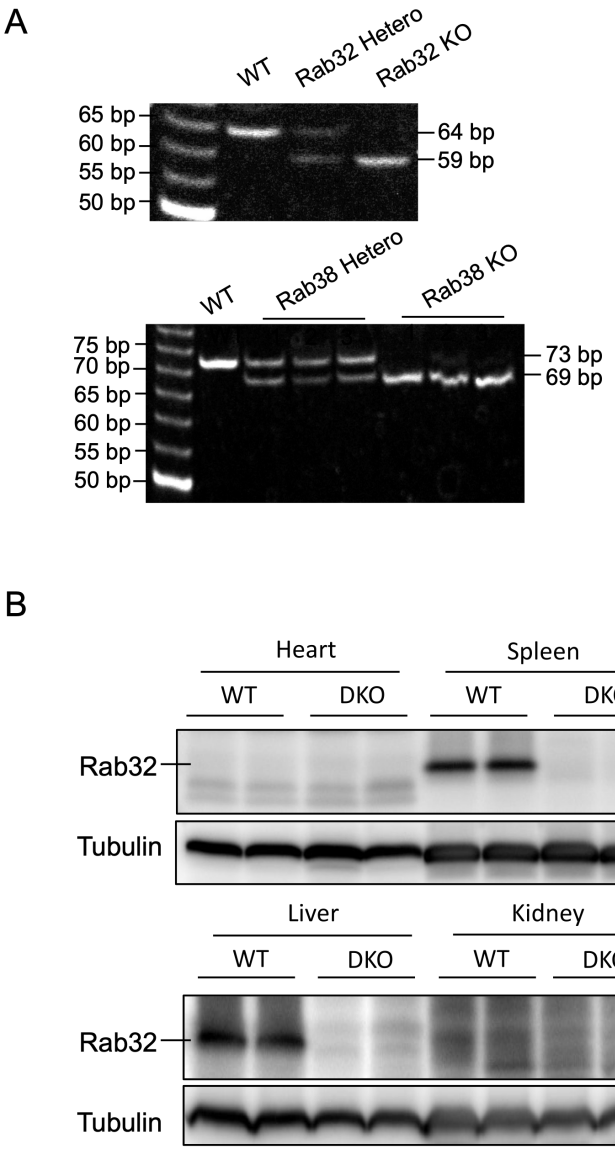

Establishment of Rab32/38 DKO mice.

(**A**) Genotyping of Rab32 and Rab38 WT and KO alleles in WT and hetero and homo mutant mice by PCR. (**B**) Two WT or Rab32/38 DKO mice were sacrificed at 8 weeks of age, and small samples of organs, including the heart, spleen, lung, liver, and kidney, were prepared for western blotting analysis using the indicated antibodies.

Figure 4

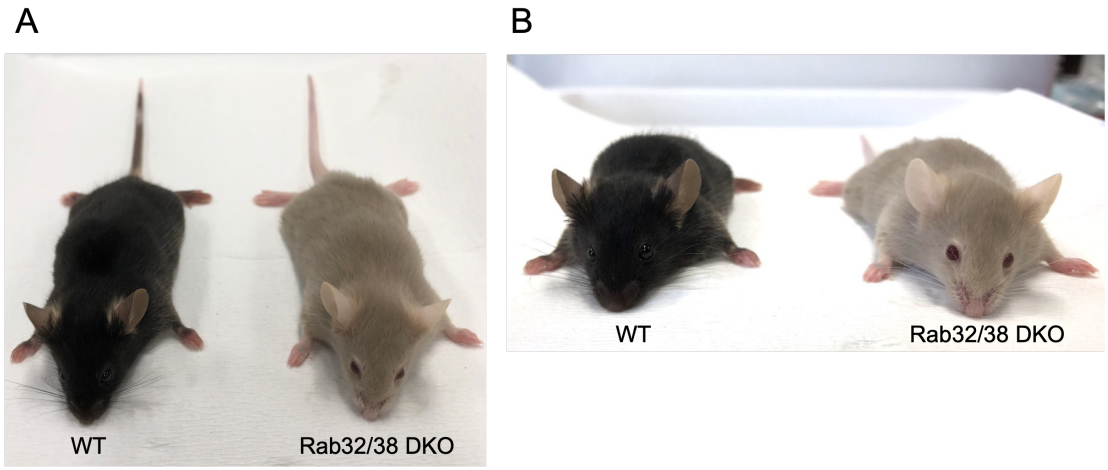

Rab32/38 DKO mice are characterized by a light beige coat and red eyes.
(**A**) Appearance of WT and Rab32/38 DKO mice. The coat color is light beige and the eye color is red in the Rab32/38 DKO mouse (Top view image). (**B**) Rab32/38 DKO mice show red eyes in compared to WT mice (Front view image).

Figure 5

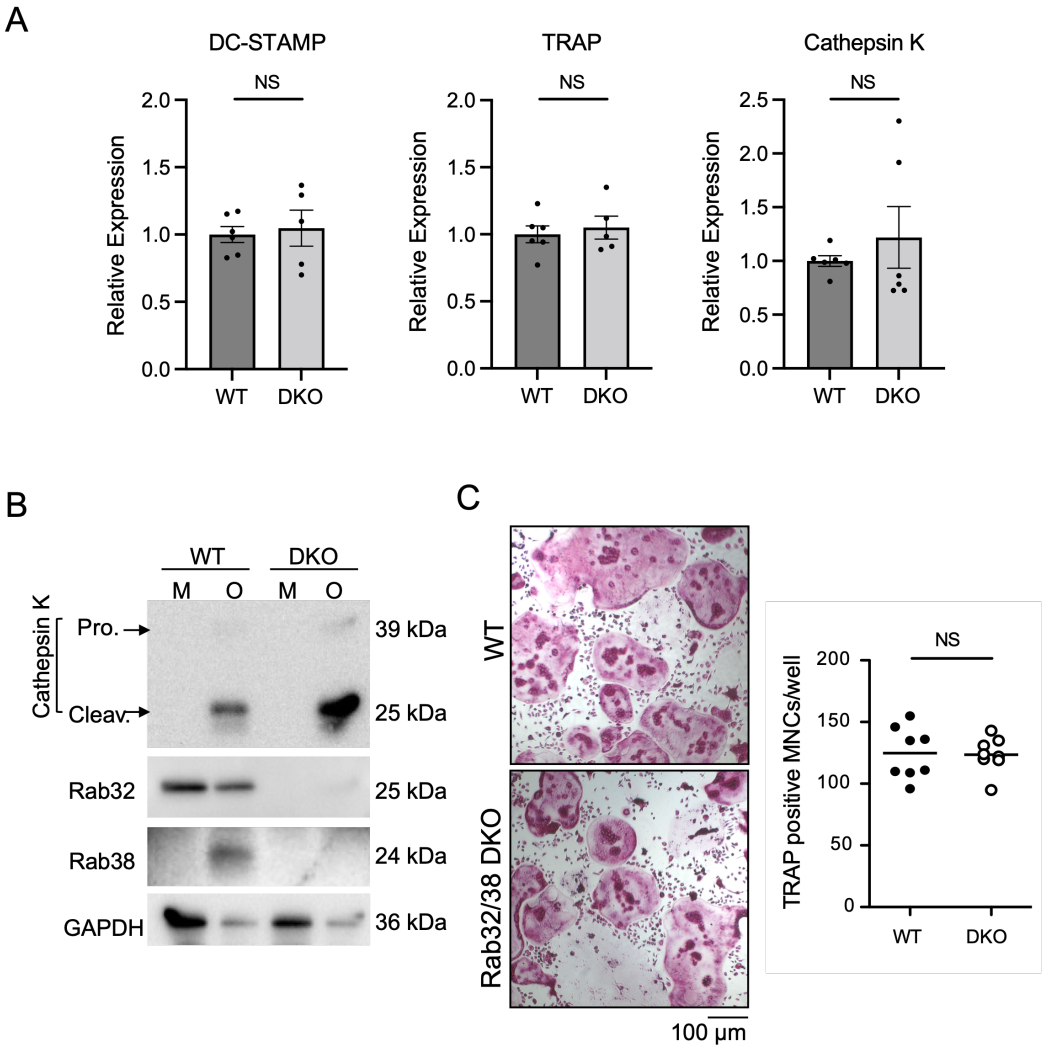

Rab32/38 DKO had no effect on osteoclast differentiation marker expression, osteoclast multinucleation, or CTSK/TRAP production.

(**A**) BMMs of WT and DKO mice were cultured in differentiation medium for 5-6 days. mRNA expression levels of each marker gene before and after cell differentiation were analyzed by qPCR. Data were normalized using GAPDH as an internal control. The mRNA level of each osteoclast marker gene was normalized to its level in BMMs, and then the fold mRNA induction was normalized to the WT value. Results were obtained in three independent experiments with two technical replicates per PCR reaction. (**B**) Cell extracts of BMMs (M) and osteoclasts (O) from WT and Rab32/38 DKO mice were subjected to western blotting with the indicated antibodies. (**C)** Quantification of TRAP-positive multinucleated cells (MNCs). After the induction of differentiation of BMMs from WT and DKO mice for 5 days, TRAP staining was performed. TRAP-positive MNCs (>3 nuclei) in each view field of microscopic images were counted (n=8). Each data point is indicated as mean ± SD. Statistical analysis was performed using the unpaired Student's

Figure 6

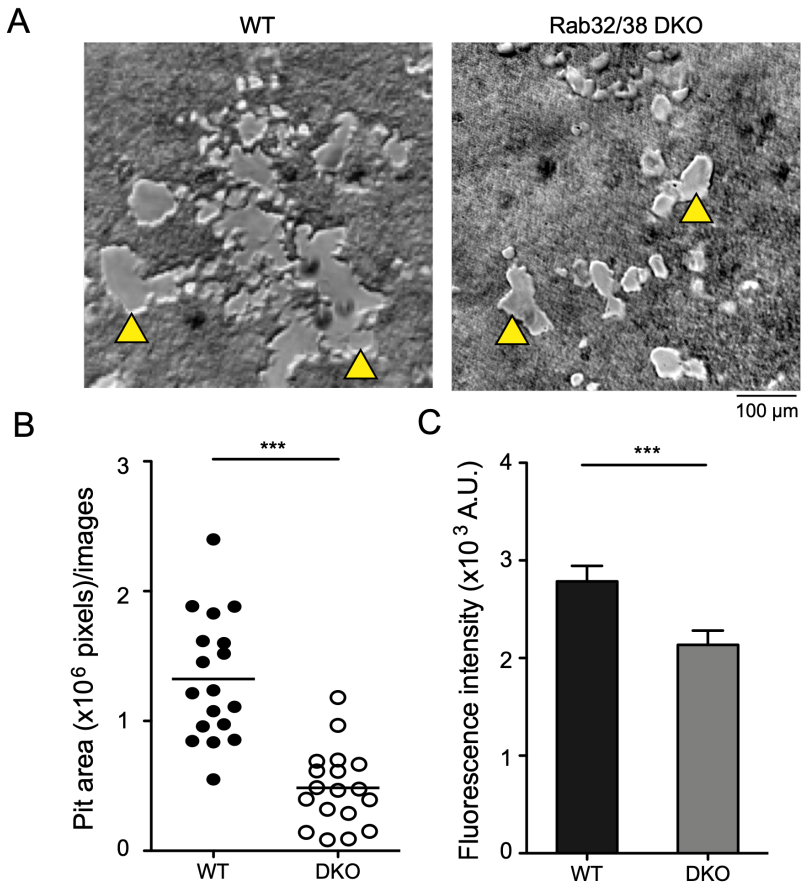

The resorptive capacity of Rab32/38 DKO–derived osteoclasts was suppressed. (**A**) Resorption pits formed by WT and Rab32/38 DKO–derived osteoclasts. Each osteoclast was cultured on a FACS-labeled calcium phosphate plate for 5 days. Resorbed areas are indicated with triangles. Scale bar: 100 μm. (**B**) The resorption pit area in Fig.6 (A) was quantified using ImageJ as described in the materials and methods. (**C**) The fluorescence intensity of culture supernatants of WT and Rab32/38 DKO–derived osteoclasts cultured on the FACS-labeled calcium phosphate plate was measured. Each data point is shown as mean ± SD. Statistical analysis was performed using the unpaired Student's t-test (* P<0.05, ** P<0.01, and *** P<0.005).

Figure 7

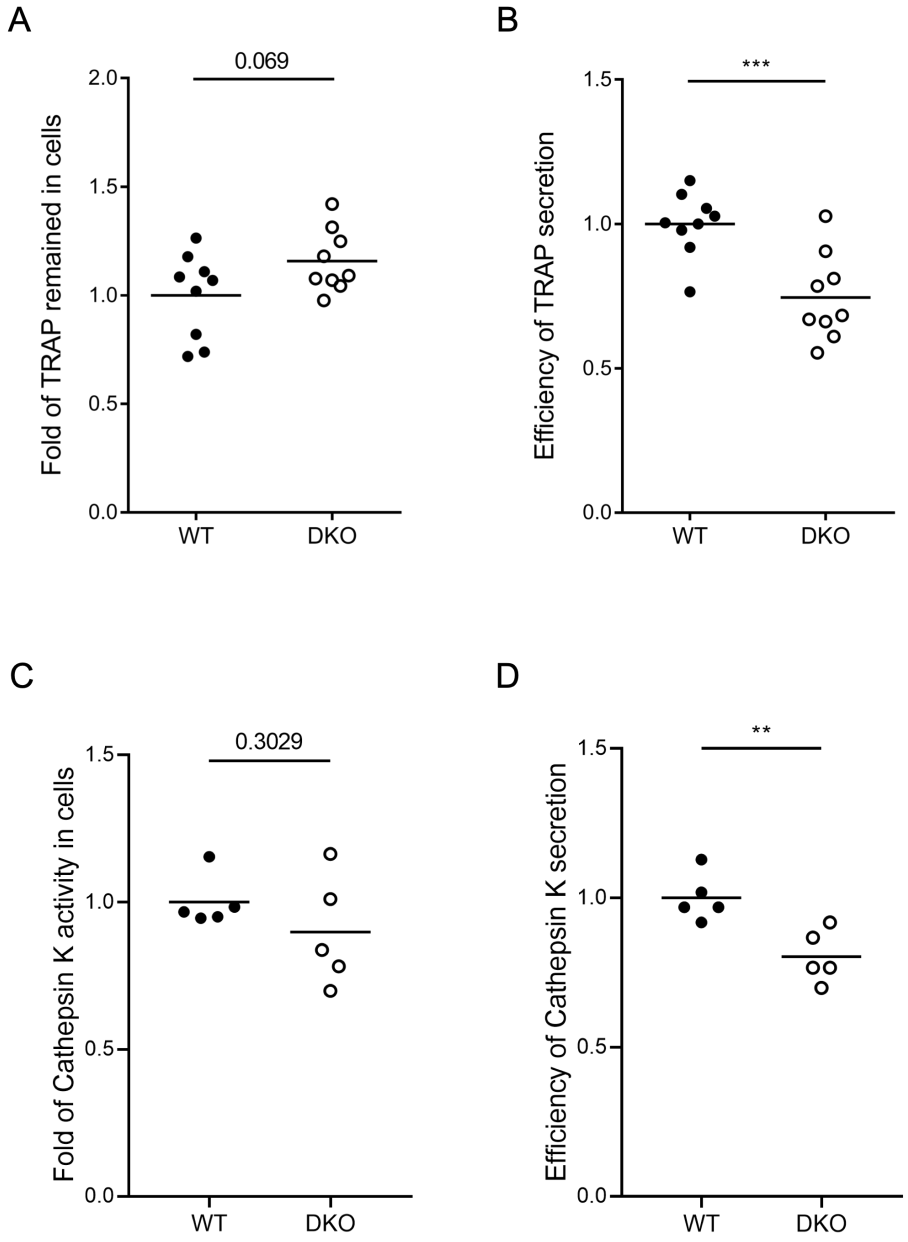

The secretion of TRAP and CTSK was decreased in osteoclasts from Rab32/Rab38 DKO mice.

(**A**) (**B**) TRAP activity in the intracellular fraction (A) and culture supernatant (B) of osteoclasts derived from WT and Rab32/38 DKO mice. (**C**) (**D**) CTSK activity in the intracellular fraction (C) and culture supernatant (D) of osteoclasts derived from WT and Rab32/38 DKO mice using the Magic Red Cathepsin K Assay Kit. Each data point is shown as mean ± SD. The analysis included 9 of 96 wells in each condition for the TRAP assay, and 5 of 24 wells in each condition for the CTSK assay. Statistical analysis was performed using the unpaired Student's t-test (* $P<0.05$, ** $P<0.01$, and *** $P<0.005$)

Figure 8

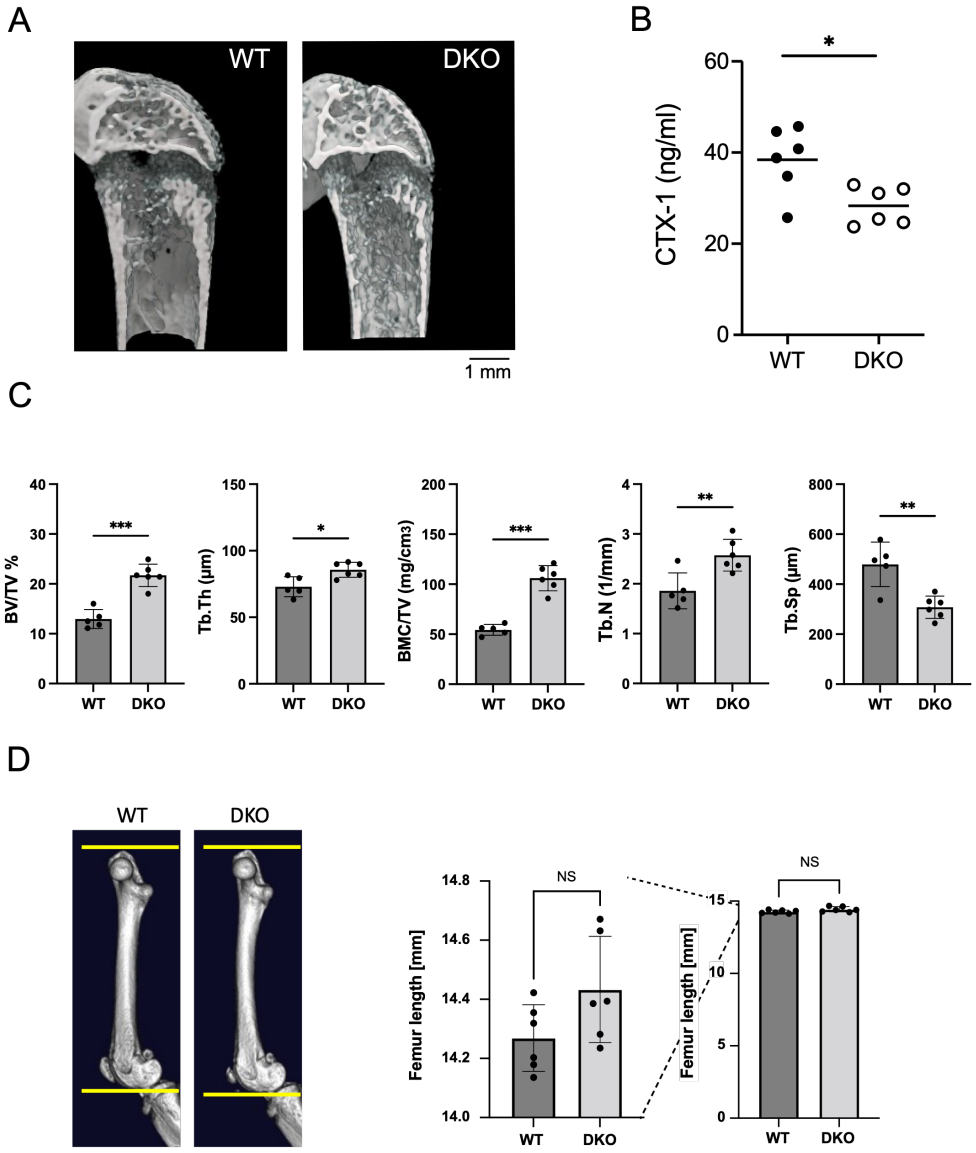

Rab32/38 DKO significantly increased trabecular bone volume in the femur. (**A**) 3D micro-CT images of femurs from 8-week-old male WT and Rab32/38 DKO mice. The Rab32/38 DKO mouse has increased trabecular bone volume due to denser bone trabeculae. Scale bar: 1 mm. (**B**) Measurement of CTX-I in the sera of 8-week-old WT and Rab32/Rab38 DKO male mice using ELISA. Each dot represents one mouse. Each data point is shown as mean ± SD. (**C**) Micro-CT analysis of the trabecular bone area in the femurs of 8-week-old male WT and Rab32/38 DKO mice. The trabecular bone structural parameters are as follows: BV/TV (%), bone volume per tissue volume; Tb. Th (μm), trabecular thickness; BMC/TV (mg/cm3), bone mineral content per trabecular bone volume; Tb. N (1/mm), trabecular number; Tb.Sp (μm), trabecular separation (n=6). (**D**) 3D micro-CT images of femurs from 8-week-old male WT and Rab32/38 DKO mice. The measured femur from the top of the caput femoris to the bottom of the condylus tibialis. Statistical analysis used the unpaired Student's t-test (* P<0.05, ** P<0.01, and *** P<0.005)

Figure 9

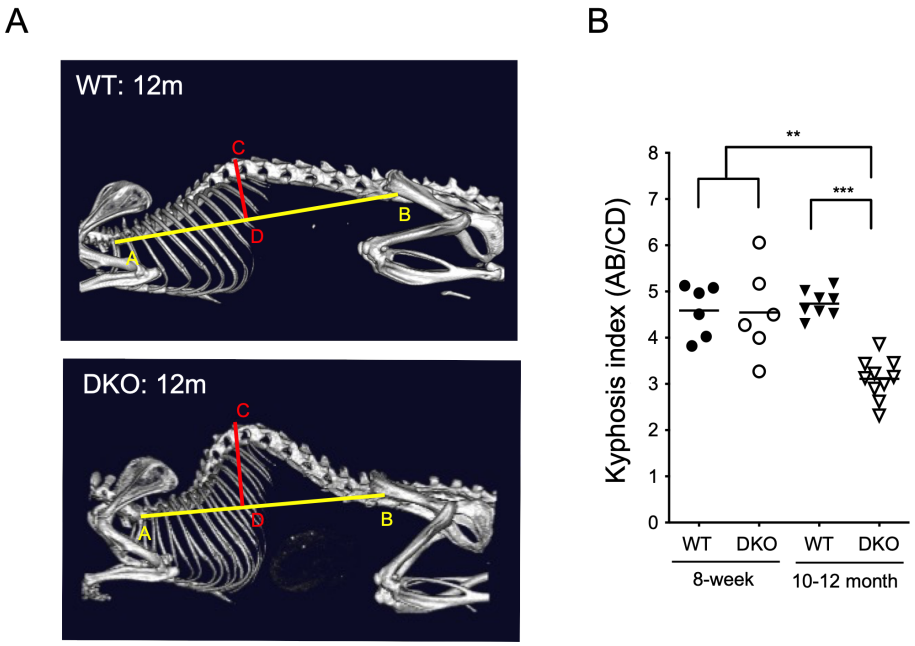

Rab32/Rab38 DKO caused bone deformation.

(**A**) Micro-CT images of the spines of 12-month-old WT and Rab32/38 DKO male mice. (**B**) The graph shows the kyphosis index (KI), defined as the distance AB divided by the distance CD from 8-week-old and 10 to 12-month-old WT and Rab32/38 DKO male mice. AB is the distance between the caudal margin of the last cervical vertebra and the caudal margin of the sixth lumbar vertebra. CD is the distance from the dorsal edge of the vertebra at the point of greatest curvature and a line perpendicular to the line AB. Each dot represents the KI of one mouse. Each data point is shown as mean ± SD. Statistical analysis used the unpaired Student's t-test (* $P<0.05$, ** $P<0.01$, and *** $P<0.005$)

8. References

1. Hadjidakis, D. J., and Androulakis, I. I. (2006) Bone Remodeling. *Ann. N. Y. Acad. Sci.* **1092**, 385–396

2. Buck, D. W., and Dumanian, G. A. (2012) Bone Biology and Physiology: Part I. The Fundamentals. *Plast. Reconstr. Surg.* **129**, 1314–1320

3. Alford, A. I., Kozloff, K. M., and Hankenson, K. D. (2015) Extracellular matrix networks in bone remodeling. *Int. J. Biochem. Cell Biol.* **65**, 20–31

4. Matsuo, K., and Irie, N. (2008) Osteoclast–osteoblast communication. *Arch. Biochem. Biophys.* **473**, 201–209

5. Florencio-Silva, R., Sasso, G. R. da S., Sasso-Cerri, E., Simões, M. J., and Cerri, P. S. (2015) Biology of Bone Tissue: Structure, Function, and Factors That Influence Bone Cells. *BioMed Res. Int.* **2015**, 1–17

6. Boyle, W. J., Simonet, W. S., and Lacey, D. L. (2003) Osteoclast differentiation and activation. *Nature*. **423**, 337–342

7. Rodan, G. A., and Martin, T. J. (2000) Therapeutic Approaches to Bone Diseases. *Science*. **289**, 1508–1514

8. Romas, E., Bakharevski, O., Hards, D. K., Kartsogiannis, V., Quinn, J. M. W., Ryan, P. F. J., Martin, T. J., and Gillespie, M. T. (2000) Expression of osteoclast differentiation factor at sites of bone erosion in collagen-induced arthritis. *Arthritis Rheum.* **43**, 821–826.

9. Teitelbaum, S. L., and Ross, F. P. (2003) Genetic regulation of osteoclast development and function. *Nat. Rev. Genet.* **4**, 638–649

10. Teitelbaum, S. L. (2000) Bone Resorption by Osteoclasts. *Science*. **289**, 1504–1508

11. Kumari, A., Silakari, O., and Singh, R. K. (2018) Recent advances in colony stimulating factor-1 receptor/c-FMS as an emerging target for various therapeutic implications. *Biomed. Pharmacother.* **103**, 662–679

12. Kim, J. H., and Kim, N. (2014) Regulation of NFATc1 in Osteoclast Differentiation. *J. Bone Metab.* **21**, 233–241

13. Takayanagi, H., Kim, S., Koga, T., Nishina, H., Isshiki, M., Yoshida, H., Saiura, A., Isobe, M., Yokochi, T., Inoue, J., Wagner, E. F., Mak, T. W., Kodama, T., and Taniguchi, T. (2002) Induction and Activation of the Transcription Factor NFATc1 (NFAT2) Integrate RANKL Signaling in Terminal Differentiation of Osteoclasts. *Dev. Cell*. **3**, 889–901

14. 須田立雄 髙橋榮明 編著 (2016) *新骨の科学 Bone Biology*, 第2版, 医歯薬出版

15. Lemma, S., Sboarina, M., Porporato, P. E., Zini, N., Sonveaux, P., Di Pompo, G., Baldini, N., and Avnet, S. (2016) Energy metabolism in osteoclast formation and activity. *Int. J. Biochem. Cell Biol.* **79**, 168–180

16. Luzio, J. P., Hackmann, Y., Dieckmann, N. M. G., and Griffiths, G. M. (2014) The Biogenesis of Lysosomes and Lysosome-Related Organelles. *Cold Spring Harb. Perspect. Biol.* **6**, a016840–a016840

17. Dell'Angelica, E. C., Mullins, C., Caplan, S., and Bonifacino, J. S. (2000) Lysosome-related organelles. *FASEB J. Off. Publ. Fed. Am. Soc. Exp. Biol.* **14**, 1265–1278

18. Stenbeck, G. (2002) Formation and function of the ruffled border in osteoclasts. *Semin. Cell Dev. Biol.* **13**, 285–292

19. Coxon, F. P., and Taylor, A. (2008) Vesicular trafficking in osteoclasts. *Semin. Cell Dev. Biol.* **19**, 424–433

20. Lacombe, J., Karsenty, G., and Ferron, M. (2013) Regulation of lysosome biogenesis and functions in osteoclasts. *Cell Cycle*. **12**, 2744–2752

21. Blott, E. J., and Griffiths, G. M. (2002) Secretory lysosomes. *Nat. Rev. Mol. Cell Biol.* **3**, 122–131

22. Stinchcombe, J., Bossi, G., and Griffiths, G. M. (2004) Linking Albinism and Immunity: The Secrets of Secretory Lysosomes. *Science*. **305**, 55–59

23. van Meel, E., Boonen, M., Zhao, H., Oorschot, V., Ross, F. P., Kornfeld, S., and Klumperman, J. (2011) Disruption of the Man-6-P Targeting Pathway in Mice Impairs Osteoclast Secretory Lysosome Biogenesis. *Traffic*. **12**, 912–924

24. Toyomura, T., Murata, Y., Yamamoto, A., Oka, T., Sun-Wada, G.-H., Wada, Y., and Futai, M. (2003) From Lysosomes to the Plasma Membrane. *J. Biol. Chem.* **278**, 22023–22030

25. Marks, M. S., Heijnen, H. F., and Raposo, G. (2013) Lysosome-related organelles: unusual compartments become mainstream. *Curr. Opin. Cell Biol.* **25**, 495–505

26. Weaver, T. E., Na, C.-L., and Stahlman, M. (2002) Biogenesis of lamellar bodies, lysosome-related organelles involved in storage and secretion of pulmonary surfactant. *Semin. Cell Dev. Biol.* **13**, 263–270

27. Pfeffer, S. R. (2017) Rab GTPases: master regulators that establish the secretory and endocytic pathways. *Mol. Biol. Cell*. **28**, 712–715

28. Homma, Y., Hiragi, S., and Fukuda, M. (2021) Rab family of small GTPases: an updated view on their regulation and functions. *FEBS J.* **288**, 36–55

29. Hutagalung, A. H., and Novick, P. J. (2011) Role of Rab GTPases in Membrane Traffic and Cell Physiology. *Physiol. Rev.* **91**, 119–149

30. Palokangas, H., Mulari, M., and Vaananen, H. K. (1997) Endocytic pathway from the basal plasma membrane to the ruffled border membrane in bone-resorbing osteoclasts. *J. Cell Sci.* **110**, 1767–1780

31. Matsumoto, N., Sekiya, M., Tohyama, K., Ishiyama-Matsuura, E., Sun-Wada, G.-H., Wada, Y., Futai, M., and Nakanishi-Matsui, M. (2018) Essential Role of the a3 Isoform of V-ATPase in Secretory Lysosome Trafficking via Rab7 Recruitment. *Sci. Rep.* **8**, 6701

32. Jo Oursler, M. (2014) The Roles of Small GTPases in Osteoclast Biology. *Orthop. Muscular Syst.* : current research, **3**, 1000161.

33. Shimada-Sugawara, M., Sakai, E., Okamoto, K., Fukuda, M., Izumi, T., Yoshida, N., and Tsukuba, T. (2015) Rab27A Regulates Transport of Cell Surface Receptors Modulating Multinucleation and Lysosome-Related Organelles in Osteoclasts. *Sci. Rep.* **5**, 9620

34. Ng, P. Y., Brigitte Patricia Ribet, A., and Pavlos, N. J. (2019) Membrane trafficking in osteoclasts and implications for osteoporosis. *Biochem. Soc. Trans.* **47**, 639–650

35. Ohbayashi, N., Fukuda, M., and Kanaho, Y. (2017) Rab32 subfamily small GTPases: pleiotropic Rabs in endosomal trafficking. *J. Biochem. (Tokyo)*. **162**, 65–71

36. Wasmeier, C., Romao, M., Plowright, L., Bennett, D. C., Raposo, G., and Seabra, M. C. (2006) Rab38 and Rab32 control post-Golgi trafficking of melanogenic enzymes. *J. Cell Biol.* **175**, 271–281

37. Tamura, K., Ohbayashi, N., Ishibashi, K., and Fukuda, M. (2011) Structure-Function Analysis of VPS9-Ankyrin-repeat Protein (Varp) in the Trafficking of Tyrosinase-related Protein 1 in Melanocytes. *J. Biol. Chem.* **286**, 7507–7521

38. Tamura, K., Ohbayashi, N., Maruta, Y., Kanno, E., Itoh, T., and Fukuda, M. (2009) Varp is a novel Rab32/38-binding protein that regulates Tyrp1 trafficking in melanocytes. *Mol. Biol. Cell*. **20**, 2900–2908

39. Oiso, N., Riddle, S. R., Serikawa, T., Kuramoto, T., and Spritz, R. A. (2004) The rat Ruby (R) locus is Rab38 : identical mutations in Fawn-hooded and Tester-Moriyama rats derived from an ancestral Long Evans rat sub-strain. *Mamm. Genome*. **15**, 307–314

40. Osanai, K., Oikawa, R., Higuchi, J., Kobayashi, M., Tsuchihara, K., Iguchi, M., Jongsu, H., Toga, H., and Voelker, D. R. (2008) A Mutation in Rab38 Small GTPase Causes Abnormal Lung Surfactant Homeostasis and Aberrant Alveolar Structure in Mice. *Am. J. Pathol.* **173**, 1265–1274

41. Huizing, M., Anikster, Y., and Gahl, W. A. (2000) Hermansky-Pudlak Syndrome and Related Disorders of Organelle Formation: Hermansky-Pudlak Syndrome. *Traffic*. **1**, 823–835

42. Aguilar, A., Weber, J., Boscher, J., Freund, M., Ziessel, C., Eckly, A., Magnenat, S., Bourdon, C., Hechler, B., Mangin, P. H., Gachet, C., Lanza, F., and Léon, C. (2019) Combined deficiency of RAB32 and RAB38 in the mouse mimics Hermansky-Pudlak syndrome and critically impairs thrombosis. *Blood Adv.* **3**, 2368–2380

43. Behnia, R., and Munro, S. (2005) Organelle identity and the signposts for membrane traffic. *Nature*. **438**, 597–604

44. Kaneko, T., and Mashimo, T. (2015) Simple Genome Editing of Rodent Intact Embryos by Electroporation. *PLOS ONE*. **10**, e0142755

45. Cohen-Solal, K. A., Sood, R., Marin, Y., Crespo-Carbone, S. M., Sinsimer, D., Martino, J. J., Robbins, C., Makalowska, I., Trent, J., and Chen, S. (2003) Identification and characterization of mouse Rab32 by mRNA and protein expression analysis. *Biochim. Biophys. Acta*. **1651**, 68–75

46. Kimura, S., Yamakami-Kimura, M., Obata, Y., Hase, K., Kitamura, H., Ohno, H., and Iwanaga, T. (2015) Visualization of the entire differentiation process of murine M cells: suppression of their maturation in cecal patches. *Mucosal Immunol.* **8**, 650–660

47. Greenblatt, M. B., Park, K. H., Oh, H., Kim, J.-M., Shin, D. Y., Lee, J. M., Lee, J. W., Singh, A., Lee, K., Hu, D., Xiao, C., Charles, J. F., Penninger, J. M., Lotinun, S., Baron, R., Ghosh, S., and Shim, J.-H. (2015) CHMP5 controls bone turnover rates by dampening NF-κB activity in osteoclasts. *J. Exp. Med.* **212**, 1283–1301

48. Mizoguchi, T., Muto, A., Udagawa, N., Arai, A., Yamashita, T., Hosoya, A., Ninomiya, T., Nakamura, H., Yamamoto, Y., Kinugawa, S., Nakamura, M., Nakamichi, Y., Kobayashi, Y., Nagasawa, S., Oda, K., Tanaka, H., Tagaya, M., Penninger, J. M., Ito, M., and Takahashi, N. (2009) Identification of cell cycle–arrested quiescent osteoclast precursors in vivo. *J. Cell Biol.* **184**, 541–554

49. Ohbayashi, N., Yatsu, A., Tamura, K., and Fukuda, M. (2012) The Rab21-GEF activity of Varp, but not its Rab32/38 effector function, is required for dendrite formation in melanocytes. *Mol. Biol. Cell*. **23**, 669–678

50. Livak, K. J., and Schmittgen, T. D. (2001) Analysis of relative gene expression data using real-time quantitative PCR and the $2^{-\Delta\Delta C_T}$ Method. *Methods San Diego Calif.* **25**, 402–408

51. Kikuta, J., Wada, Y., Kowada, T., Wang, Z., Sun-Wada, G.-H., Nishiyama, I., Mizukami, S., Maiya, N., Yasuda, H., Kumanogoh, A., Kikuchi, K., Germain, R. N., and Ishii, M. (2013) Dynamic visualization of RANKL and Th17-mediated osteoclast function. *J. Clin. Invest.* **123**, 866–873.

52. Usami, Y., Gunawardena, A. T., Francois, N. B., Otsuru, S., Takano, H., Hirose, K., Matsuoka, M., Suzuki, A., Huang, J., Qin, L., Iwamoto, M., Yang, W., Toyosawa, S., and Enomoto-Iwamoto, M. (2019) Possible Contribution of Wnt-Responsive Chondroprogenitors to the Postnatal Murine Growth Plate. *J. Bone Miner. Res.* **34**, 964–974

53. Cardiff, R. D., Miller, C. H., and Munn, R. J. (2014) Manual Hematoxylin and Eosin Staining of Mouse Tissue Sections. *Cold Spring Harb. Protoc. Cold Spring Harb. Prot.* **2014**, 655-658.

54. Loftus, S. K., Larson, D. M., Baxter, L. L., Antonellis, A., Chen, Y., Wu, X., Jiang, Y., Bittner, M., Hammer, J. A., and Pavan, W. J. (2002) Mutation of melanosome protein RAB38 in chocolate mice. *Proc. Natl. Acad. Sci. U. S. A.* **99**, 4471–4476

55. Saftig, P., Hunziker, E., Wehmeyer, O., Jones, S., Boyde, A., Rommerskirch, W., Moritz, J. D., Schu, P., and von Figura, K. (1998) Impaired osteoclastic bone resorption leads to osteopetrosis in cathepsin-K-deficient mice. *Proc. Natl. Acad. Sci.* **95**, 13453–13458

56. Yagi, M., Miyamoto, T., Sawatani, Y., Iwamoto, K., Hosogane, N., Fujita, N., Morita, K., Ninomiya, K., Suzuki, T., Miyamoto, K., Oike, Y., Takeya, M., Toyama,

Y., and Suda, T. (2005) DC-STAMP is essential for cell–cell fusion in osteoclasts and foreign body giant cells. *J. Exp. Med.* **202**, 345–351

57. Minkin, C. (1982) Bone acid phosphatase: Tartrate-resistant acid phosphatase as a marker of osteoclast function. *Calcif. Tissue Int.* **34**, 285–290

58. Garnero, P., Ferreras, M., Karsdal, M., Nicamhlaoibh, R., Risteli, J., Borel, O., Qvist, P., Delmas, P., Foged, N., and Delaissé, J. (2003) The Type I Collagen Fragments ICTP and CTX Reveal Distinct Enzymatic Pathways of Bone Collagen Degradation. *J. Bone Miner. Res.* **18**, 859–867

59. Grunewald, M., Kumar, S., Sharife, H., Volinsky, E., Gileles-Hillel, A., Licht, T., Permyakova, A., Hinden, L., Azar, S., Friedmann, Y., Kupetz, P., Tzuberi, R., Anisimov, A., Alitalo, K., Horwitz, M., Leebhoff, S., Khoma, O. Z., Hlushchuk, R., Djonov, V., Abramovitch, R., Tam, J., and Keshet, E. (2021) Counteracting age-related VEGF signaling insufficiency promotes healthy aging and extends life span. *Science*. **373**, eabc8479

60. Laws, N., and Hoey, A. (2004) Progression of kyphosis in *mdx* mice. *J. Appl. Physiol.* **97**, 1970–1977

61. Charles, J. F., Coury, F., Sulyanto, R., Sitara, D., Wu, J., Brady, N., Tsang, K., Sigrist, K., Tollefsen, D. M., He, L., Storm, D., and Aliprantis, A. O. (2012) The collection of NFATc1-dependent transcripts in the osteoclast includes numerous genes non-essential to physiologic bone resorption. *Bone*. **51**, 902–912

62. Chen, X., Wang, Z., Duan, N., Zhu, G., Schwarz, E. M., and Xie, C. (2018) Osteoblast–osteoclast interactions. *Connect. Tissue Res.* **59**, 99–107

63. Bultema, J. J., Boyle, J. A., Malenke, P. B., Martin, F. E., Dell'Angelica, E. C., Cheney, R. E., and Di Pietro, S. M. (2014) Myosin Vc interacts with Rab32 and

Rab38 proteins and works in the biogenesis and secretion of melanosomes. *J. Biol. Chem.* **289**, 33513–33528

64. Tabata, H., Kawamura, N., Sun-Wada, G.-H., and Wada, Y. (2008) Vacuolar-type H+-ATPase with the a3 isoform is the proton pump on premature melanosomes. *Cell Tissue Res.* **332**, 447–460

65. Sun-Wada, G.-H., Tabata, H., Kawamura, N., Aoyama, M., and Wada, Y. (2009) Direct recruitment of H+-ATPase from lysosomes for phagosomal acidification. *J. Cell Sci.* **122**, 2504–2513

66. Zhao, H., Laitala-Leinonen, T., Parikka, V., and Väänänen, H. K. (2001) Downregulation of Small GTPase Rab7 Impairs Osteoclast Polarization and Bone Resorption. *J. Biol. Chem.* **276**, 39295–39302

67. Matsumoto, N., Sekiya, M., Sun-Wada, G.-H., Wada, Y., and Nakanishi-Matsui, M. (2022) The lysosomal V-ATPase a3 subunit is involved in localization of Mon1-Ccz1, the GEF for Rab7, to secretory lysosomes in osteoclasts. *Sci. Rep.* **12**, 8455

68. Harkema, L., Youssef, S. A., and de Bruin, A. (2016) Pathology of Mouse Models of Accelerated Aging. *Vet. Pathol.* **53**, 366–389

69. Kuperus, J. S., Mohamed Hoesein, F. A. A., de Jong, P. A., and Verlaan, J. J. (2020) Diffuse idiopathic skeletal hyperostosis: Etiology and clinical relevance. *Best Pract. Res. Clin. Rheumatol.* **34**, 101527

70. Halloran, B. P., Ferguson, V. L., Simske, S. J., Burghardt, A., Venton, L. L., and Majumdar, S. (2002) Changes in Bone Structure and Mass With Advancing Age in the Male C57BL/6J Mouse. *J. Bone Miner. Res.* **17**, 1044–1050

71. Ferguson, V. L., Ayers, R. A., Bateman, T. A., and Simske, S. J. (2003) Bone development and age-related bone loss in male C57BL/6J mice. *Bone*. **33**, 387–398

72. Mumtaz, H., Dallas, M., Begonia, M., Lara-Castillo, N., Scott, J. M., Johnson, M. L., and Ganesh, T. (2020) Age-related and sex-specific effects on architectural properties and biomechanical response of the C57BL/6N mouse femur, tibia and ulna. *Bone Rep.* **12**, 100266

73. Almeida, M., Laurent, M. R., Dubois, V., Claessens, F., O'Brien, C. A., Bouillon, R., Vanderschueren, D., and Manolagas, S. C. (2017) Estrogens and Androgens in Skeletal Physiology and Pathophysiology. *Physiol. Rev.* **97**, 135–187

74. Stone, J. A., McCrea, J. B., Witter, R., Zajic, S., and Stoch, S. A. (2019) Clinical and translational pharmacology of the cathepsin K inhibitor odanacatib studied for osteoporosis. *Br. J. Clin. Pharmacol.* **85**, 1072–1083

75. Russell, R. G. G. (2011) Bisphosphonates: The first 40years. *Bone*. **49**, 2–19

9. Acknowledgments

I am greatly thankful to Prof. Takeshi Noda of the Department of Advanced Oral Biology, Center for Frontier Oral Science, Graduate School of Dentistry, Osaka University, for giving me the opportunity to conduct my research as my advisor and for his great research guidance and support. I would also like to deeply thank assistant Professor Dr. Shiou-Ling Lu of the Noda laboratory for her help in my research and for always supporting me with warm words.

Also, I am grateful to Dr. Siyu Chen and Ms. Zhang Zidi, members of Noda laboratory, for their help in supporting experiments; Dr Kazuya Noda, Dr. Shintaro Kira and Dr. Yohei Yamamoto for their advice and help with experimental design; Dr. Sumiko Ikari and Dr. Yi Zhou for their help with mouse management; Dr. Katsutoshi Hirose, Dr. Yu Usami and Dr. Satoru Toyosawa of the Department of Oral Pathology, Graduate School of Dentistry, Osaka University for the opportunity to have guidance and discussion on micro-CT analysis and pathological analysis of bones of mice; Dr. Mitsunori Fukuda of Department of Integrative Life Sciences, Graduate School of Life Sciences, Tohoku University, Dr. Shinya Murakami of Department of Periodontology, Graduate School of Dentistry, Osaka University, Dr. Ge-Hong Sun-Wada of Department of Biochemistry, Faculty of Pharmaceutical Sciences, Doshisha Women's College and Dr. Yoh Wada of Department of Biological Sciences, Institute of Scientific and Industrial Research, Osaka University for materials and technical advices.

I am grateful to Dr. Sunao Takeshita at the National Institute for Longevity Sciences for providing CMG14-12 cells, and Dr. Shunsuke Kimura at the Graduate School of Pharmaceutical Sciences, Keio University for providing the GST-RANKL constructed plasmid; Dr. Tomoji Mashimo and Mr. Yoshihiro Uno of the Institute of

Experimental Animal Sciences, Graduate School of Medicine, Osaka University, for the generation of Rab32/38 DKO F_0 mice.

Finally, I am truly grateful to my family and friends who have supported me for a long time.

10. Achievements

10.1. Publications

1. Kanako Tokuda, Shiou-Ling Lu, Siyu Chen, Kazuya Noda, Katsutoshi Hirose, Yu Usami, Shinya Murakami, Satoru Toyosawa, Mitsunori Fukuda, Ge-Hong Sun-Wada, Yoh Wada, Takeshi Noda: Rab32 and Rab38 facilitate osteoclast function by regulating the intracellular traffic of acid hydrolases and V-ATPase.（After the first submission to JBC, under preparation in response to the reviewer‘s comments planning for resubmission）
2. Kazuya Noda, Siyu Chen, Shiou-Ling Lu, Kanako Tokuda, Feike Hao, Yoh Wada, Ge-Hong Sun-Wada, Shinya Murakami, Mitsunori Fukuda, Takashi Itoh, Takeshi Noda: Characterization of Rab32- and Rab38-positive lysosome-related organelles in osteoclasts and macrophages. （Under review after resubmission in response to minor comments in JBC）
3. Siyu Chen, Shiou-Ling Lu, Kazuya Noda, Kanako Tokuda, Hiroko Omori, Nao Shikata, Chao-Yuan Tsai, Hitoshi Kikutani, Mitsunori Fukuda, Shinya Murakami, Takeshi Noda: Mitochondrial autophagy is exclusively carried out by microautophagy in macrophages. （Under preparation）

10.2. Meetings

1. **Kanako Tokuda**, Kazuya Noda, Yo-hei Yamamoto, Yu Usami, Katsutoshi Hirose, Satoru Toyosawa, Mitsunori Fukuda, Takeshi Noda, The analysis of Rab32/38

mediated membrane traffic in macrophage and osteoclast, 2019 ASCB|EMBO Meeting, (Washington D.C., December7-11, 2019)

2. **徳田加奈子**、野田和也、山本洋平、宇佐美悠、豊澤悟、福田光則、野田健司, マウス骨組織における Rab32/38 の機能解析, 第 92 回日本生化学会大会（横浜,2019 年 9 月 19 日）
3. **徳田加奈子**、野田和也、山本洋平、宇佐美悠、福田光則、野田健司, 破骨細胞における Rab32/38 を介した新規細胞内膜動態の解析, 第 41 回日本分子生物学会年会（横浜, 2018 年 11 月 30 日）
4. **徳田加奈子**、呂旸菱、陳思禹、野田和也、廣瀬勝俊、宇佐美悠、村上伸也、豊澤悟、福田光則、和田戈虹、和田洋、野田健司, Rab32 と Rab38 は酸加水分解酵素と V-ATPase の細胞内輸送を制御することにより破骨細胞の機能を促進する, 第 95 回日本生化学会大会（名古屋, 2022 年 11 月 11 日）
5. 陳思禹、呂旸菱、野田和也、**徳田加奈子**、大森弘子、福田光則、和田洋、村上伸也、野田健司, マクロファージにおけるミトファジーは主にミクロオートファジーが担う, 第 95 回日本生化学会大会（名古屋, 2022 年 11 月 11 日）